Available online at www.sciencedirect.com
SCIENCE DIRECT
Lithos 89 (2006) 405–423
LITHOS
www.elsevier.com/locate/lithos

Origin of layered continental mantle (Karelian craton, Finland): Geochemical and Re–Os isotope constraints

Petri Peltonen [a,*], Gerhard Brügmann [b]

[a] Geological Survey of Finland, P.O. Box 96, FI-02151 Espoo, Finland
[b] Max-Planck-Institut für Chemie, Postfach 3060, D-55020 Mainz, Germany

Received 27 June 2005; accepted 27 December 2005
Available online 4 April 2006

Abstract

Studies of mantle xenolith and xenocryst studies have indicated that the subcontinental lithospheric mantle (SCLM) at the Karelian Craton margin (Fennoscandian Shield) is stratified into at least three distinct layers cited A, B, and C. The origin and age of this layering has, however, remained unconstrained. In order to address this question, we have determined Re–Os isotope composition and a comprehensive set of major and trace elements, from xenoliths representing all these three layers. These are the first Re–Os data from the SCLM of the vast East European Craton.

Xenoliths derived from the middle *layer B* (at ~110–180 km depth), which is the main source of harzburgitic garnets and peridotitic diamonds in these kimberlites, are characterised by unradiogenic Os isotopic composition. $^{187}Os/^{188}Os$ shows a good correlation with indices of partial melting implying an age of ~3.3. Ga for melt extraction. This age corresponds with the oldest formation ages of the overlying crust, suggesting that layer B represents the unmodified SCLM stabilised during the Paleoarchean. Underlying *layer C* (at 180–250 km depths) is the main source of Ti-rich pyropes of megacrystic composition but is lacking harzburgitic pyropes. The osmium isotopic composition of layer C xenoliths is more radiogenic compared to layer B, yielding only Proterozoic T_{RD} ages. Layer C is interpreted to represent a melt metasomatised equivalent to layer B. This metasomatism most likely occurred at ca. 2.0 Ga when the present craton margin formed following continental break-up. Shallow *layer A* (at ~60–110 km depth) has knife-sharp lower contact against layer B indicative of shear zone and episodic construction of SCLM. Layer A peridotites have "ultradepleted" arc mantle-type compositions, and have been metasomatised by radiogenic $^{187}Os/^{188}Os$, presumably from slab-derived fluids. Since layer A is absent in the core of the craton, its origin can be related to Proterozoic processes at the craton margin. We interpret it to represent the lithosphere of a Proterozoic arc complex (subduction wedge mantle) that became underthrusted beneath the craton margin crust during continental collision ~1.9 Ga ago.

Keywords: Rhenium; Osmium; Isotopic composition; Mantle; Peridotite; Karelian craton; Fennoscandia, Finland

1. Introduction

Deciphering the events that have led to the stabilisation of the lithospheric mantle beneath Archean cratons, and the subsequent reworking processes remains a challenging task. Isotopic systems often show open behaviour at the ambient pressure–temperature conditions within the stability field of garnet peridotites, or are seriously disturbed by mantle metasomatism. The rhenium–osmium isotope systematic may be less prone to such a disturbance and the system has been

* Corresponding author.
E-mail address: petri.peltonen@gtk.fi (P. Peltonen).

0024-4937/$ - see front matter © 2006 Elsevier B.V. All rights reserved.
doi:10.1016/j.lithos.2005.12.013

successfully applied to obtain age information on the depletion history and stabilisation of deep cratonic roots. Data have become available from the major Archean cratons of southern Africa, Siberia, USA, and Canada (Walker et al., 1989; Pearson et al., 1995a; Olive et al., 1997; Chesley et al., 1999; Meisel et al., 2001; Pearson et al., 2002; Irvine et al., 2003; Carlson et al., 2004). In this study, we present the first Re–Os data from the mantle beneath the Fennoscandian Shield, more specifically of mantle xenoliths derived from the roots of the Archean Karelian craton by 600 Ma old kimberlite magmatism. In fact, our Re–Os data are the first to be reported from the lithospheric mantle of the whole East European Craton, the vast, largely unexposed Archean–Proterozoic terrain extending from the Ural Mountains through the Black Sea to the North Atlantic.

Dating of the mantle events that have led to the present architecture and composition of the Karelian cratonic root is particularly interesting for several reasons. First, the Karelian craton seems to represent the oldest one of several Archean microcontinents that form the Karelia–Kola craton. The oldest crustal orthogneisses have yielded crystallisation ages of ~3550 Ma, and U–Pb ages for inherited zircons provide evidence for the existence of even older, up to 3700 Ma old, protocrust (Mutanen and Huhma, 2003). Similar ages have been obtained by single grain zircon U–Pb dating of mafic lower crustal xenoliths found in the same kimberlites as the mantle peridotites analysed in this study. These xenoliths record crystallisation ages of up to 3500 Ma, with Nd model ages providing evidence of an even older protolith (~3700 Ma; Peltonen et al., in press). Together, these data indicate that the Karelian craton crust represents one of the first continental nuclei that emerged on the early Earth, and that its upper and lower crust have probably remained coupled since the Paleoarchean.

Whether the lithospheric mantle–and to what extent–has remained coupled with the crust since their stabilisation is a fundamental question concerning the preservation of the first continental landmasses on the Earth. Our samples come from lithospheric mantle at the craton margin. Earlier studies have indicated that the lithospheric mantle at this locality has a layered structure, comprising at least three compositionally distinct layers (Peltonen et al., 1999; Lehtonen et al., 2004). To constrain the origin of such layering and the "age" relationship between these layers is of prime importance to our understanding of the geodynamic evolution of this craton margin.

2. Outline of the Karelian Craton

The Karelian craton forms a coherent, mainly late Archean cratonic nucleus ~400 000 km^2 in size in eastern and northern Finland and adjacent Russia (Fig. 1). Approximately 1/3 of the Karelian Craton is buried under Phanerozoic sedimentary deposits of the Russian Platform. In the southeast, beneath these cover deposits, Karelian Craton terminates within the Meso-Neoproterozoic central Russian aulagogens and rifts, a zone that parallels the Paleoproterozoic suture zone between the Archean of Fennoscandia and Volgo-Uralia (Bogdanova et al., 2005). In the northeast, the Karelian craton is bordered by the Belomoridian belt, that has been interpreted to represent the NE edge of the Karelian craton that became thermally reworked during the Lapland-Kola orogen ~1.9–1.8 Ga (Skiöld et al., 2001).

The Archean of the Karelian Craton mainly consists of banded tonalite–trondhjemite–granodiorite (TTG) gneisses, greenstone belts, and with lesser abundance of migmatitic (para)gneisses and diorite–granodiorite–granite plutons. The craton includes at least 16 NNW-trending greenstone belts. Case studies have proposed distinct origins for individual belts: oceanic plateau for the Kostomuksha (Puchtel et al., 1998), island arc for the Sumozero–Kenozero (Puchtel et al., 1999) and continental rift zone origin for the Kuhmo–Suomussalmi belt (Luukkonen, 1992). Together with considerable internal differences between individual gneiss-granite terrains, such diverse settings imply a complex–so far poorly constrained–accretionary history during the Archean. Most of the greenstone belts and TTG series gneisses were formed between 2.70 and 2.85 Ga, with a smaller population of ages clustering at ~3.1–3.2 Ga (for a review see: Sorjonen-Ward and Luukkonen, 2005). More recently, Mutanen and Huhma (2003) and Peltonen et al. (in press) have reported U–Pb zircon and T_{DM}(Nd) model ages of the order of 3.5–3.7 Ga from upper and lower crustal samples, respectively, suggesting that Karelian Craton includes terrains that represent some of the oldest continental crust on Earth.

Layered intrusions, dyke swarms and lava fields record discrete events of cratonic extension at 2.45, 2.3, 2.2, 2.1 and 1.97 Ga (Vuollo, 1994). Some uncertainty exists whether it was the ~2.1 or ~1.97 Ga event that led to continental break-up, and formation of the passive nonvolcanic margin at the present southwest margin of the craton (Nironen, 1997). The present structure of the craton margin is the result of the accretion of two juvenile arc complexes to the cratonic nucleus between

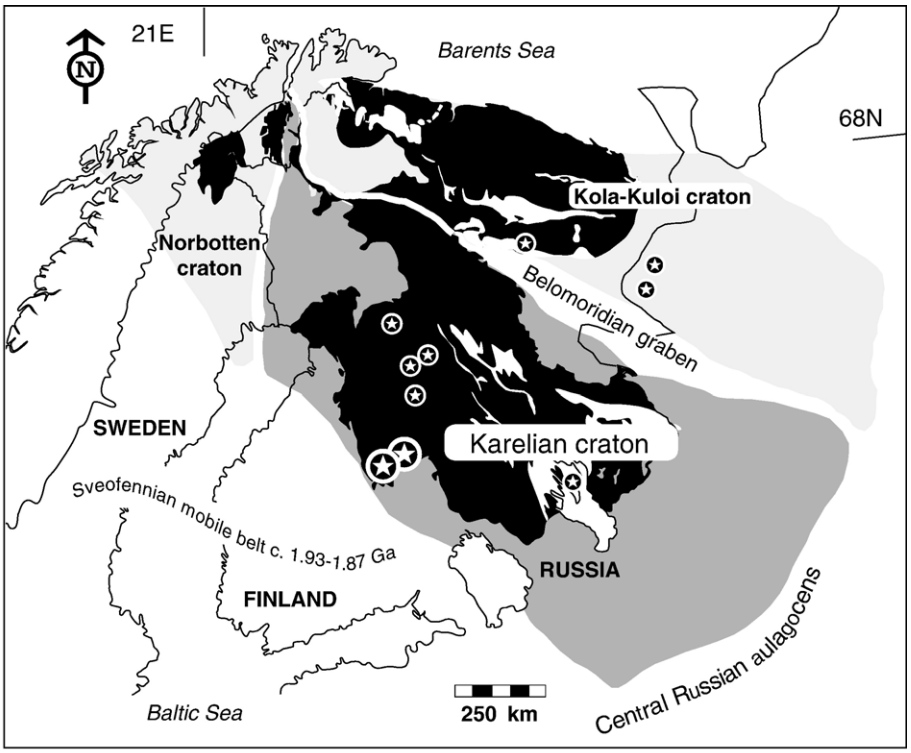

Fig. 1. Generalised geological map showing the extent of the three Archean subcratons, Kola, Karelia, and Norbotten, which together make up the Archean of the Fennoscandia. Black shading refers to the exposed Archean crust while grey denotes the Archean crust that is covered by younger supracrustal rocks or that has been reworked during the Proterozoic. Kaavi-Kuopio kimberlites are indicated by a large star; other known kimberlite occurrences by smaller symbol.

1.91 and 1.87. This event caused tectono-thermal overprinting and shattering of the craton margin basement into several megablocks (Sorjonen-Ward and Luukkonen, 2005).

3. Layered Karelian lithosphere

Previous studies of mantle xenoliths have shown that the lithospheric mantle beneath the Kaavi-Kuopio kimberlite province is structurally and compositionally stratified. Based on the petrology of mantle xenoliths, Peltonen et al. (1999) subdivided the lithospheric mantle into two distinct layers: (1) shallow, strongly depleted and modally metasomatised layer that consists of fine grained garnet-spinel harzburgites. This upper mantle layer is underlain by a more fertile layer (2), consisting of coarse garnet lherzolites, harzburgites, wehrlites and minor eclogites, extending down to the base of the lithosphere. Later, this layered structure has been characterised in more detail by analysing large number of pyropic garnet xenocrysts from the kimberlites (Lehtonen et al., 2004). Xenocryst data imply that the lower lithospheric layer can be further subdivided into two compositionally distinct layers. Thus, the whole lithospheric column consists of three distinct layers, from now on called layers A, B and C. These layers, summarised in depth vs. TiO_2(gt)-diagram in Fig. 2, have the following characteristics.

Layer A extends from c. 60 km to ~ 110 km depth. This zone is characterised by pyropic garnets that are extremely depleted in Ti, Zr, and Y. Meanwhile, they are high in Ca, a feature that is poorly understood, but their decoupled trace and major elements contents probably indicate an origin through exsolution from former high-*T*/high-*P* orthopyroxene (Lehtonen, 2005). Five fine-grained garnet-spinel harzburgite xenoliths have similar garnet compositions and represent larger samples from this layer. Two spinel facies xenoliths originated from the narrow garnet-free layer between the shallowest garnet xenocrysts and the Moho at ~ 60 km depth, and are also included in layer A.

Layer B extends from 110 to 180 km. It is defined by the depth interval where ultradepleted Ca-rich garnets do not exist anymore, but which instead is characterised by the presence of low-Ca and high-Cr harzburgitic garnets. Most of the xenocrysts in kimberlites are

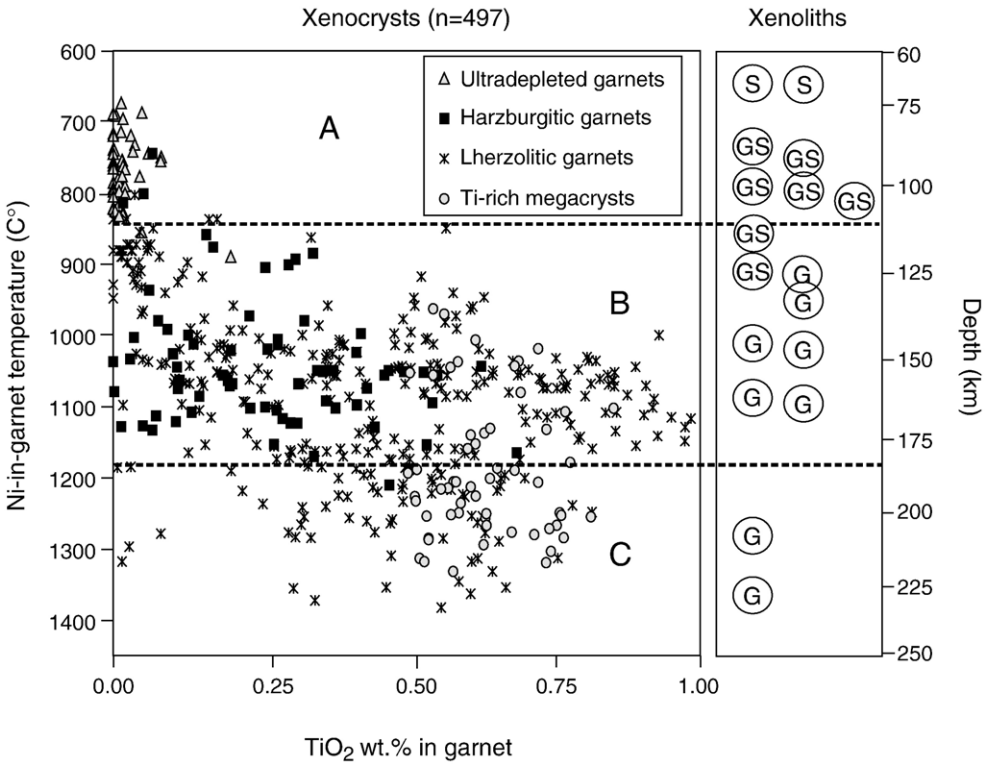

Fig. 2. TiO_2 content of garnet xenocryst vs. depth of equilibration. Depth for each pyrope grain was constrained by projecting the Ni-in-garnet temperature of Ryan et al. (1996) onto the local geotherm (modified after Lehtonen et al., 2004). Xenocryst data reveal several, compositionally distinct, layers (A, B, and C) within the continental mantle. Layer A is characterised by ultradepleted garnet compositions, layer B by subcalcic harzburgitic ("diamond indicator") garnets and a large compositional range, while layer C is more fertile containing no strongly depleted garnets. Instead, layer C is the main source of relatively TiO_2-rich garnets of megacrysts composition (classification after Schulze, 2003). In order to relate the xenolith data to these xenocryst-based layers, the depth of the origin for each xenolith was determined with the same method, and is indicated on the right side of the diagram. S, GS, and G refer to spinel-, garnet-spinel, and garnet facies peridotite xenoliths, respectively. Spinel facies xenoliths originate from the garnet-free "window" between the depth of the Moho and that of the shallowest garnet xenocrysts.

derived from this layer. The TiO_2 contents of pyropes from layer B are highly variable indicating a larger degree of lithological diversity compared to other layers. This feature is also evident in the variable modal composition of xenoliths, which include harzburgites, lherzolites, wehrlites and some websterites.

The lowermost *layer C* extends from 180 km to the base of the lithosphere at ~250 km. This layer is characterised by the absence of subcalcic harzburgitic garnets and lherzolitic pyropes are less depleted compared to those of layer B. Furthermore, layer C is characterised by the presence of abundant orange, relatively Cr-poor and Ti–Zr–Y-rich, pyropes of megacrysts composition (Lehtonen et al., 2004). Importantly, the B–C boundary does not represent the lithosphere–asthenosphere boundary because all mantle xenoliths from layer C still have coarse textures, with no evidence of shearing. In addition to peridotites, layer C also contains diamondiferous eclogites, believed to occur as thin stretched layers or small pods among the layer C peridotites (Peltonen et al., 2002).

4. Samples

The Kaavi-Kuopio kimberlites, which have chemical and isotopic composition similar to the Group I kimberlites–particularly similar to those of Koidu, west Africa–are found at two clusters, located only ~30 and ~50 km inwards from the westernmost margin of the craton, respectively. Chemical and isotopic compositions of these kimberlites have been extensively discussed by O'Brien and Tyni (1999). Nineteen fresh or only weakly serpentinised peridotite xenoliths from these pipes were available for this study. Other mantle material recovered from these pipes includes rare orthopyroxenites and eclogite xenoliths, and many megacrysts and xenocrysts. Xenolith samples were recovered during an extensive search along several

kilometres of drill core material from 19 kimberlite pipes. Mantle xenoliths are present in each pipe but when hosted by tuffisitic kimberlite facies they are invariably strongly altered and not suitable for geochemical study. Four of the pipes (#2, #5, #9, #14) contain basaltic kimberlite facies rocks with fresh mantle xenoliths. Some mineralogical and geochemical data for seven of these samples were reported already by Peltonen et al. (1999), but full analyses are also reported in this study for the sake of completeness. Selected petrographic and mineral chemical information is summarised in Table 1. Full mineral analyses can be obtained from the first author upon request.

With respect to their aluminium-bearing phase, the studied samples represent three peridotite facies: spinel peridotites (4), garnet-spinel peridotites (7) and garnet peridotites (8). Thus, they clearly represent a considerable range of depths of origin. Our aim is to relate the chemical and isotope data of these xenoliths with the xenocryst-determined mantle layers described above. In order to make the xenocryst and xenolith depths comparable, the *P–T* conditions for the xenoliths were determined by analysing the Ni-contents of the garnets. To bring out any systematic vertical variations in the Re–Os isotope ratios and model ages of the Karelian mantle, all but four of the smallest samples were analysed for Re–Os isotopes. These samples cover all rock textures as well as the whole compositional spectrum with respect to indices of partial melting, such as the Al_2O_3 content, and trace element abundances.

We also analysed three host kimberlite samples, representing pipes #1, #2, and #14, for Re–Os isotopes. Full chemical analyses of 30 kimberlite samples, including the 3 re-analysed here, can be found in O'Brien and Tyni (1999). These kimberlites have typical Group I mineralogy, major and trace element and isotopic compositions and intrusion morphologies (O'Brien and Tyni, 1999). Hypabyssal samples with low Contamination Index (C.I.; Clement, 1982) were selected for Re–Os analyses in order to analyse kimberlites as primitive as possible. Furthermore, on the basis of platinum-group element analyses (unpublished), we pre-selected samples with variable Os content in order to constrain the source of Os in the kimberlite.

5. Petrography of the samples

5.1. Spinel and garnet-spinel facies peridotites

Most of the spinel-bearing peridotite xenoliths also contain garnet. Their Ni-in-garnet temperatures range between 750 °C and 914 °C which constrain their origin within the xenocryst-determined layer A and uppermost layer B. Thus, the facies boundary between spinel-bearing and spinel-free peridotites does not coincide with a compositional boundary in the continental mantle (Fig. 2). Spinel-bearing xenoliths are granuloblastic rocks being generally finer grained than garnet peridotites (below). They are all strongly depleted in their basaltic constituents: two of the samples are dunites the remaining being harzburgites, which by definition contain ≤ 5 vol.% of clinopyroxene. Three of the samples are completely devoid of clinopyroxene, and at least some of the clinopyroxene in the other samples is likely to be of post-melting in origin (Peltonen et al., 1999; Lehtonen, 2005). Some of the samples, especially the fine-grained ones, bear petrographic evidence for modal metasomatism in the form of minor (<0.2%) secondary flaky phlogopite and interstitial amphibole (magnesio-katophorite).

5.2. Garnet facies peridotites

Garnet peridotite nodules differ from spinel-bearing samples in several respects. They are all "coarse" in texture. They are generally more fertile and show wider a range of modal compositions than spinel-bearing samples. In order of abundance they are lherzolites, harzburgites or wehrlites. Two of the samples show minor 20–200-μm-size olivine neoblast formation, and approach porphyroclastic textures. Sheared samples are not present. Undulatory extinction of olivine and pyroxene is ubiquitous. Garnet is generally well preserved and sometimes rimmed by kelyphite that consists of intergrown grains of clinopyroxene, brown euhedral spinel, and phlogopite. In one garnet harzburgite sample (#5.8/74), most of the garnet has been replaced by the mineral assemblage clinopyroxene −orthopyroxene−spinel−phlogopite−carbonate. Several garnet facies xenoliths contain trace amounts of ilmenite, which is generally present as euhedral 100-μm-size inclusions in garnet. Garnet-facies xenoliths do not bear evidence of modal metasomatism.

5.3. Kimberlite samples

Three samples representing pipes #1, #2, and #14 were analysed for their Re–Os isotopes. These pipes are oval to oblate in shape, and 0.5 to 1.5 ha in size. Samples represent hypabyssal kimberlite. Their matrix consists of monticellite microphenocrysts, perovskite, zoned chromite, calcite, serpentine, and kinoshitalite mica. They also display the classic suite of lithospheric

Table 1
Key parameters for mantle xenolith and kimberlite samples from Kaavi-Kuopio kimberlites, Finland

Sample no.	Lithology	Pipe no.	Ti garnet (ppm)	Ni garnet (ppm)	T Ni [a]	Depth (km)	Layer	Modal compositions						Mineral chemistry			
								Ol	Cpx	Opx	Gt	Spi	Flo	Opx Mg#	Cpx Mg#	Gt Mg#	Fo olivine
14.4/38.70	spi harzburgite	14	–	–	–	70	A	80.0	–	17.0	–	3		0.921	–	–	91.550
14.7/66.65	spi harzburgite	14	–	–	–	70	A	88.0	0.1	11.0	–	+	+	0.930	–	–	92.250
9.2/24.37	gt-spi harzburgite	9	56	17	750	92	A	76.8	0.5	19.0	3.0	0.5		0.927	0.955	0.798	91.820
14.4/30.55	gt-spi harzburgite	14	119	19	775	96	A	82.0	–	10.0	8.0	+	+	0.923	–	0.782	91.230
9.2/31.46	gt-spi harzburgite	9	15	20	784	98	A	67.8	4.4	20.6	6.1	+		0.928	0.951	0.792	91.910
Lu5-15-8/84.10	gt-spi harzburgite	5	1	22	811	103	A	71.7	–	22.4	5.8	1	+	0.929	–	0.815	91.694
14.7./44.48	gt-spi harzburgite	14	17	22	814	104	A	79.0	1.2	15.4	3.2	+		0.925	0.939	0.792	91.700
R18-38.45B	gt-spi harzburgite	2	39	27	861	113	B	85.0	1.8	7.8	5.4	1		0.931	0.950	0.805	91.967
Lu5-15-4/37.80	gt-spi harzburgite	5	84	34	914	123	B	94.1	–	3.6	1.7	1		0.938	–	0.830	92.611
14.01/11.5	gt-harzburgite	14	207	33	909	122	B	60.7	3.6	32.4	3.2			0.935	0.935	0.846	92.350
R18-40.50	gt-lherzolite	2	1571	38	946	130	B	85.4	7.0	4.1	3.3				0.895	0.769	87.726
R18-33.45	gt-lherzolite	2	2577	50	1030	147	B	84.3	7.2	6.4	1.9			0.925	0.920	0.827	91.053
R18-38.45A	gt-lherzolite	2	527	52	1042	150	B	66.2	8.4	10.4	14.8			0.921	0.917	0.824	90.678
R18-37.05	gt-harzburgite	2	770	62	1100	163	B	80.4	–	16.2	3.2			0.933	–	0.832	92.318
Lu5-15-2/35.95	gt-lherzolite	5	3233	63	1108	164	B	68.2	7.6	11.2	12.8		+	0.936	0.933	0.859	92.673
5.8/84.85	gt-lherzolite	5	1676	96	1281	206	C	57.4	9.6	25.2	7.7			0.920	0.914	0.841	90.820
5.8/74	gt-harzburgite	5	2882	120	1389	234	C	68.6	–	23.5	7.9			0.920	–	0.838	90.820
R18-45.65	dunite+res spi	2	–	–	–	< 120	A?	98.0	–	–	–	2		–	–	–	91.247
Ju11-8-7/34.15	dunite+res spi	14	–	–	–	< 120	A?	90.5	1.7	4.3	–	1	1.5	0.929	0.917	–	91.688
			C.I. [b]	McrOl % [c]													
2.150/11.6–12.0	kimberlite	2	1.42	< 5													
1.107/16.95	kimberlite	1	0.98	15–25													
14.05/39.05–39.32	kimberlite	14	1.12	15–25													

[a] Calibration of Ryan et al. (1996).
[b] C.I. = Contamination index of Clement (1982).
[c] Modal content of macrocrystal olivine.

mantle-derived xenocrysts: olivine, red to purple pyrope, Mg-ilmenite, Cr–Al spinel, and bright green Cr-diopside. Samples show variable olivine contents. Olivine has a trimodal size distribution with abundant 0.1–0.4 size grains mostly interpreted as phenocrysts (Fo_{83-86}), 1–5 mm sized rounded macrocrysts (Fo_{89-93}), and occasional cm sized megacrysts (Fo_{90}).

6. Analytical techniques

Xenoliths were detached from the drill core and pealed off any visible alteration rims by thin-bladed diamond saw. Samples were cut into thin slices and pulverised in a carbon steel bowl tested to be free of any PGE. Major elements were determined from fused $LiBO_3$ beads by XRF using a Philips PW 1480 sequential wavelength dispersive spectrometer. All trace elements, except Re and Os, were determined by ICP-MS (Perkin-Elmer Sciex Elan 5000) at the Geological Survey of Finland. For ICP-MS trace element analyses samples were dissolved in a mixture of hydrofluoric and perchloric acids, evaporated, and redissolved in nitric acid. To ensure total decomposition of the sample, the solution was filtered, the filter ashed and fused with 0.2 g of lithium metaborate and 0.02 g sodium metaborate, followed by dissolution of the fused bead in nitric acid and combination with the filtrate.

For Re–Os analysis approximately 2 g (peridotites) or 3 g (kimberlites) of sample powder was digested in a quartz tube together with a Re–Os isotope tracer (^{185}Re, ^{190}Os), 4 ml conc. HCl and 6 ml conc. HNO_3, for 16 h in a high-pressure asher at ca. 100 bar and 300 °C. Osmium was separated from all sample solutions by solvent extraction with bromine and purified by microdistillation (Birck et al., 1997). Os and Re isotope measurements and Os concentrations were performed by N-TIMS with a Finnigan MAT 262 mass spectrometer, and Re concentrations were analysed by isotope dilution using the multicollector ICP-MS at the Max-Planck-Institut für Chemie, Mainz, Germany.

Major element compositions of minerals were determined by the wavelength dispersive mode (WDS) using Cameca Camebax SX50 instrument at the GSF. Acceleration voltage of 25 kV, probe current of 50 nA, and beam diameter of 10 μm were applied. Standards included both natural and synthetic minerals and data reduction was made using the PAP correction procedure supplied by Cameca. Trace Ni, Mn, and Ti data by EPM were obtained on pyrope grains employing 500-nA probe current, 600-s counting times on peak plus background positions, and were reduced by the CSIRO TRACE program for the SX50 (Robinson and Graham, 1992). Crosschecking has indicated that by such methodology EPM can achieve similar precision to that of LA-ICP-MS down to the level of ~ 10 ppm for Ni, Mn, and Ti (Lehtonen et al., 2004).

7. Results

7.1. Ni-in-garnet thermometry

Nickel-in-garnet temperatures were obtained for each garnet-bearing xenolith by substituting the Ni concentrations (Table 2) in to the thermometer calibration of Ryan et al. (1996). To obtain equilibration pressure, the obtained Ni-in-garnet temperatures were projected onto the Karelian craton geotherm of Kukkonen and Peltonen (1999). This references geotherm has been determined for the same locality by applying geothermobarometry of mantle xenoliths and heat flow constraints. Pressures (in kb) were then converted to depth Z (in km) according to equation $Z=(P-13.7)*3.092+50$. The depths reported here (Table 2) differ from those reported earlier for some of the same samples due to the application of other thermobarometry calibrations (Kukkonen and Peltonen, 1999). The absolute PT values are, however, not critical for our purpose, which is to obtain comparable PT estimates for pyrope xenocrysts and xenoliths. Nickel-in-garnet temperatures are not available for spinel peridotite xenoliths. Their depth of origin is, however, tightly constrained: the stability of spinel peridotite extends from the Moho depth (at ~60 km; Korsman et al., 1999) to that of the origin of shallowest garnet xenocryst (~ 80 km depth; Lehtonen et al., 2004). Hence, we have arbitrarily defined a depth of 70 km to our garnet-free spinel peridotite xenoliths. These estimates can be compared with data from the Kaapvaal craton, where Boyd et al. (1999) report that the garnet-in boundary lies at ca. 100 km depth.

The approximate locus of origin for each xenolith with respect to layers as determined by xenocryst mapping is indicated in Fig. 2. Importantly, despite of the abundance of subcalcic harzburgitic garnets among xenocrysts, such garnets are not present in xenoliths, suggesting that lithologies which contain harzburgitic garnets (garnet dunites and harzburgites) are more breakable during kimberlite transport.

7.2. Major and trace element composition of the mantle xenoliths

Peridotite nodules from Kaavi-Kuopio kimberlites (Table 2) have chemical compositions broadly similar to those derived from Kaapvaal and Siberian cratonic roots

Table 2
Major and trace element abundances in the mantle xenolith and kimberlite samples from Kaavi-Kuopio kimberlites, Finland

Sample no.	Lithology	Layer	SiO_2	TiO_2 [a]	Al_2O_3	Fe_2O_3	MgO	MnO	CaO	Na_2O	K_2O	P_2O_5	S	Cr	Ni	Co	Sc	Ti [c]	V	Zn	Cu	Ga
14.4/38.70	spi-harzburgite	A	41.00	<0.02	0.61	8.46	46.60	0.12	0.39	<0.08	0.13	0.03	n.a.	2380	2720	114	6.68	14.1	32.1	43.5	8.78	0.53
14.7./66.65	spi harzburgite	A	41.78	0.02	0.22	8.53	47.26	0.12	0.19	0.09	0.09	<0.014	4.31	1870	2290	112	4.31	44.9	27.7	54	10.80	0.52
9.2./24.37 [b]	gt-spi harzburgite	A	43.92		0.77	8.28	46.69		0.34				2.18	1660	2260	109	2.18	253	35.5	47.1	5.00	0.77
14.4/30.55	gt-spi harzburgite	A	41.80	0.07	0.83	9.20	45.50	0.13	0.46	0.16	0.19	0.02	n.a.	2170	2230	115	6.67	311	32.1	66.3	5.72	1.05
9.2./31.46	gt-spi harzburgite	A	42.98	0.01	1.00	8.52	44.05	0.13	0.92	0.12	0.13	0.02	12.8	2240	2140	105	12.8	20	47	44.6	<5	0.74
Lu5-15-8/84.10 [b]	gt-spi harzburgite	A	44.65		1.28	8.34	45.23		0.51				n.a.	2530	2180	105	6.87	432	41.1	29.1	26.00	<0.2
14.7/44.48	gt-spi harzburgite	A	42.67	0.10	0.26	9.07	44.12	0.12	0.63	0.14	0.24	0.05	3.76	1410	2070	105	3.76	457	33	44.9	8.96	0.7
R18-38.45B	gt-spi harzburgite	B	39.50	0.03	1.09	7.99	42.80	0.11	0.77	<0.08	0.04	0.03	n.a.	3030	2420	111	12.5	200	42.9	37.5	11.50	1.44
Lu5-15-4/37.80	gt-spi harzburgite	B	38.90	0.03	0.25	7.02	40.70	0.07	0.15	<0.08	<0.03	0.02	n.a.	1480	2450	107	1.61	165	22.2	36.4	1.59	0.54
14.01/11.5	gt-harzburgite	B	46.59	0.04	0.84	7.59	41.42	0.11	1.01	0.15	0.09	0.02	n.a.	1160	1870	90	6.28	124	34	47.6	6.61	0.98
R18-40.50	gt-lherzolite	B	40.50	0.16	1.08	10.00	37.00	0.11	2.97	0.21	0.13	0.07	n.a.	1630	1750	109	11.4	942	91.7	48.2	72.5	3.39
R18-33.45	gt-lherzolite	B	40.40	0.08	0.83	8.29	42.10	0.10	0.97	0.13	0.06	0.04	n.a.	1740	2600	121	8.50	517	48.0	44.2	5.02	1.11
R18-38.45A	gt-lherzolite	B	41.50	0.11	2.22	8.60	38.20	0.11	2.13	0.20	0.05	0.03	n.a.	1880	2380	117	13.7	667	73.4	45.7	11.70	2.21
R18-37.05	gt-harzburgite	B	40.10	0.04	0.44	7.39	41.20	0.07	0.34	<0.08	0.03	0.03	n.a.	1690	2510	109	5.48	204	30.5	32.9	4.43	0.44
Lu5-15-2/35.95	gt-lherzolite	B	41.90	0.19	3.55	6.94	38.00	0.13	2.80	0.19	0.05	0.03	n.a.	4520	2070	96	19.0	1150	101	39.6	62.60	2.09
5.8./84.85	gt-lherzolite	C	42.99	0.06	2.29	8.85	39.87	0.13	1.55	0.10	0.02	<0.014	13.9	2120	1860	97	13.9	263	55.3	66.5	8.14	1.69
5.8./74	gt-harzburgite	C	44.22	0.07	1.15	8.77	42.42	0.13	0.72	0.09	0.02	<0.014	9.5	2030	1970	103	9.5	304	39.6	53.7	6.44	1.33
R18-45.65	dunite+res spi	A?	38.20	0.01	0.17	9.16	46.80	0.10	0.05	<0.08	<0.03	0.02	n.a.	455	2890	138	4.98	38.9	<0.5	43.4	6.04	0.30
Ju11-8-7/34.15	dunite+res spi	A?	39.80	0.09	0.62	8.34	44.80	0.12	0.51	0.16	0.39	0.07	n.a.	1360	2290	109	3.16	508	28.2	47.7	8.77	0.34
2.150/11.6–12.0	kimberlite		32.08	2.34	5.43	11.79	22.58	0.26	10.09	0.10	1.95	0.60	400	1171	599	59.9	173	n.a.	173	84	119.0	n.a.
1.107/16.95	kimberlite		25.56	1.52	3.07	11.28	29.05	0.23	16.07	0.13	0.11	0.60	1100	1438	906	63.8	17.8	n.a.	112	78	110.0	n.a.
14.05/39.05–39.32	kimberlite		34.96	2.84	3.48	11.49	29.96	0.19	3.78	0.14	2.27	0.34	600	1334	1027	78.2	16.8	n.a.	155	78	119.0	n.a.

n.a. = not analysed.

[a] Ti analyses by XRF.

[b] Major element abundances calculated from the mineral modes and mineral compositions.

[c] Ti analyses by ICP-MS.

Sample no.	Rb	Sr	Ba	Nb	Ta	Y	Zr	Hf	U	Th	Pb	La	Ce	Pr	Nd	Sm	Eu	Gd	Tb	Dy	Ho	Er	Yb
14.4/38.70	6.23	36.1	n.a.	2.45	0.09	0.13	0.78	<0.5	0.05	0.17	2.22	1.49	2.16	0.17	0.63	0	0.04	0.09	0.01	0.04	<0.1	0.03	0.03
14.7./66.65	3.07	25.3	29.50	6	0.13	0.14	2.41	n.a.	<0.1	0.23	n.a.	1.77	3.07	0.29	0.92	0.12	0.05	0.10	<0.02	0.10	<0.02	0.10	<0.05
9.2./24.37[b]	4.2	51.7	45.30	6.99	0.8	0.27	4.6	n.a.	0.15	0.43	n.a.	3.03	4.78	0.44	1.45	0.25	0.05	0.10	<0.02	0.10	<0.02	0.10	<0.05
14.4/30.55	9.17	29.6	n.a.	3.62	0.15	0.19	1.46	<0.5	0.12	0.25	1.12	1.9	2.98	0.27	0.88	0.17	0.12	0.13	0.04	0.07	<0.1	0.06	0.07
9.2./31.46	5.01	46.2	45.9	2.83	0.12	0.18	2.74	n.a.	0.13	0.32	n.a.	2.37	3.88	0.38	1.06	0.15	<0.05	<0.1	<0.02	<0.1	<0.02	<0.1	0.06
Lu5-15-8/84.10[b]	2.81	7.63	36.20	2.50	0.22	0.18	4.14	<0.5	<0.2	<0.5	0.40	1.90	2.94	0.26	1.05	0.38	0.18	0.65	<0.1	0.32	<0.1	0.15	0.21
14.7/44.48	9.65	81.7	115	10.1	0.46	0.21	1.1	n.a.	0.25	0.43	n.a.	5.82	8.54	0.78	2	0.24	0.05	0.15	0.02	<0.1	<0.02	<0.1	<0.05
R18-38.45B	2.35	26.2	35.20	3.58	<0.2	0.42	<0.5	<0.5	<0.2	<0.5	<0.4	1.95	2.55	0.26	0.90	<0.2	0.10	0.15	<0.1	0.10	<0.1	0.17	<0.15
Lu5-15-4/37.80	0.75	9.96	14.70	1.96	<0.2	<0.1	<0.5	<0.5	<0.2	<0.5	0.86	1.28	1.74	0.18	0.57	<0.2	0.10	0.15	<0.1	0.10	<0.1	0.15	<0.15
14.01/11.5	3.19	32.3	31.5	3.14	0.2	0.28	3.15	n.a.	<0.1	0.41	n.a.	2.27	3.81	0.38	1.41	0.19	<0.05	0.11	0.02	<0.1	<0.02	<0.1	<0.05
R18-40.50	9.73	59.8	65.2	7.01	0.39	0.94	3.91	<0.5	<0.2	0.58	0.52	4.39	7.99	0.83	3.29	0.42	0.11	0.43	<0.1	0.19	<0.1	<0.15	<0.15
R18-33.45	3.67	21.5	18.20	1.91	<0.2	0.39	0.87	<0.5	<0.2	<0.5	<0.4	1.38	1.68	0.21	0.48	<0.2	0.10	0.16	<0.1	0.12	<0.1	0.15	<0.15
R18-38.45A	3.68	30.5	70.10	5.42	0.29	1.23	2.77	<0.5	<0.2	<0.5	<0.4	3.13	5.34	0.59	1.98	0.20	0.10	0.29	<0.1	0.12	<0.1	0.17	0.16
R18-37.05	2.09	11.7	389.0	2.09	<0.2	0.23	<0.5	<0.5	<0.2	<0.5	<0.4	1.36	1.90	0.18	0.67	<0.2	0.10	0.15	<0.1	0.10	<0.1	0.15	<0.15
Lu5-15-2/35.95	5.08	39.7	156.0	1.38	<0.2	3.55	10.0	<0.5	<0.2	<0.5	3.32	1.81	2.56	0.26	1.38	0.26	0.26	0.71	<0.1	0.48	0.10	0.49	0.56
5.8./84.85	1.06	17.9	88.40	1.37	0.14	1.12	7.8	n.a.	<0.1	0.25	n.a.	1.16	2.18	0.25	0.79	0.18	0.06	0.10	0.03	0.21	0.04	0.12	0.18
5.8./74	1.06	8.66	20.10	0.8	0.08	0.74	2.54	n.a.	<0.1	0.14	n.a.	0.67	1.33	0.15	0.41	<0.1	0.05	0.10	<0.02	0.11	0.03	0.10	0.07
R18-45.65	0.49	5.44	4.68	0.69	<0.2	<0.1	<0.5	<0.5	<0.2	<0.5	<0.4	0.28	0.48	<0.1	<0.2	<0.2	<0.1	<0.15	<0.1	<0.1	<0.1	<0.15	<0.15
Ju11-8-7/34.15	18.2	78.9	156	7.87	0.36	0.37	3.98	<0.5	0.21	<0.5	0.86	4.14	7.19	0.74	2.43	0.27	<0.1	0.20	<0.1	0.11	<0.1	<0.15	<0.15
2.150/11.6–12.0	100.0	890	1523	205	11	13.8	94.4	2.30	3.92	19.2	7.82	141	237	23.5	76.1	9.45	2.16	6.37	0.74	2.89	0.47	1.15	0.92
1.107/16.95	10.3	1240	2687	233	13	8.6	62.6	1.52	3.79	26.7	9.92	174	287	26.7	83.3	8.92	1.67	5.56	0.61	1.91	0.29	0.77	0.53
14.05/39.05–39.32	86.2	457	1254	177	12	9.2	63.7	2.07	2.79	16.4	8.62	100	171	17.3	53.4	6.66	1.60	4.95	0.54	2.01	0.34	0.72	0.58

(e.g. Boyd et al., 1999; Canil, 2004). Major element compositional trends are summarised in selected Harker diagrams in Fig. 3. Generally, analyses form reasonable trends between the most depleted samples and the composition of the primitive mantle (pyrolite). These data suggest that peridotite samples contain variable amounts of basaltic component, either due to variable degree of melt extraction from fertile protoliths, or–alternatively–due to variable degree of refertilisation by melt ingress. The spinel-bearing xenoliths from layers A are clearly the most depleted and show only a narrow range in the indices of partial melting, such as Al_2O_3 content (0.22–1.00 wt.%). Garnet peridotites, representing layers B and C, show wider range and generally more fertile compositions, consistent with their lherzolitic nature. Among the major elements, potassium is an exception: the abundances are highest in the most depleted samples implying preferential addition of potassium to the most depleted protoliths.

Moderately incompatible trace elements, e.g. Ti, Sc, V, and Ga show particularly well-defined trends between the endmember compositions of dunite xenoliths and primitive mantle (Fig. 4). Compatible trace elements, Ni and Co bring out some difference between the B and other mantle layers: B layer seems to have higher Ni and Co abundances at a given MgO or Al_2O_3 content. Incompatible trace elements Rb, Sr, Nb and LREE, show similar behaviour as potassium. Their abundances generally exceed that of primitive upper mantle. Identical trace element patterns, together with Rb–Sr and Sm–Nd whole rock isotopic ratios with host kimberlites, suggest that up to few percent kimberlite-like melt or fluid has metasomatised the xenoliths. Isotopic disequilibria between whole rocks and mineral separates imply that metasomatism occurred during emplacement or only shortly before that (Peltonen et al., 1999).

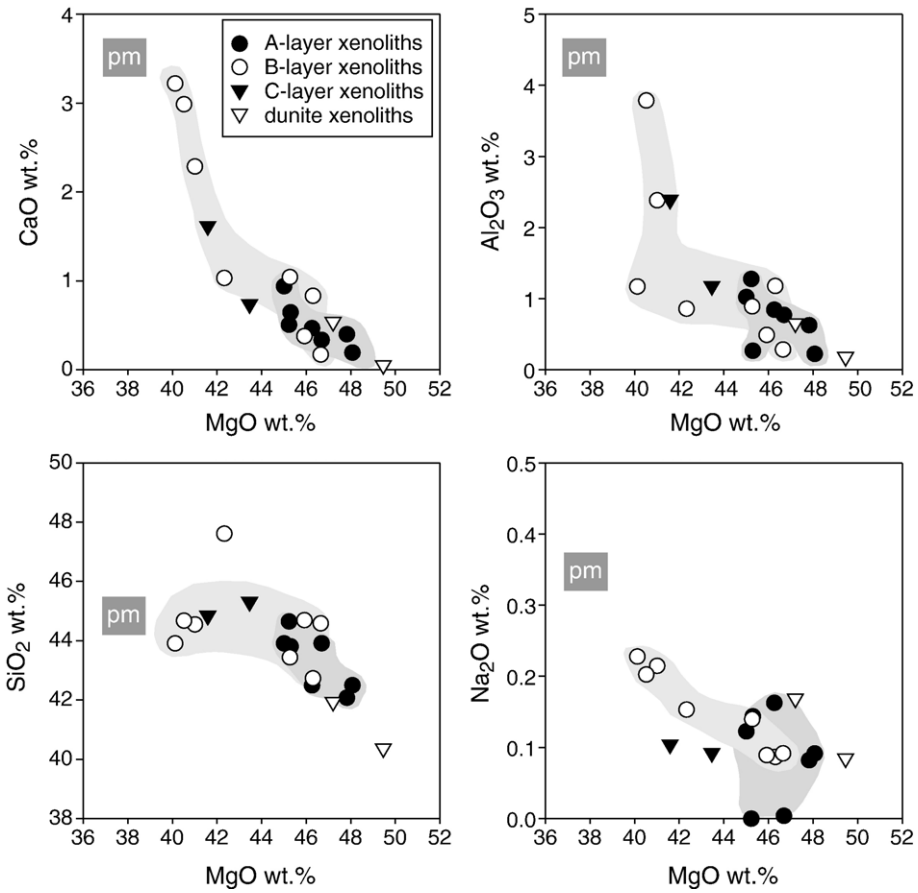

Fig. 3. Selected major element plots for the xenolith samples studied. Note the large compositional range–especially within the B-layer samples–and well-defined trends suggesting variable degrees of partial melting as the main cause of the observed compositional range. PM is primitive mantle estimate of McDonough and Sun (1995).

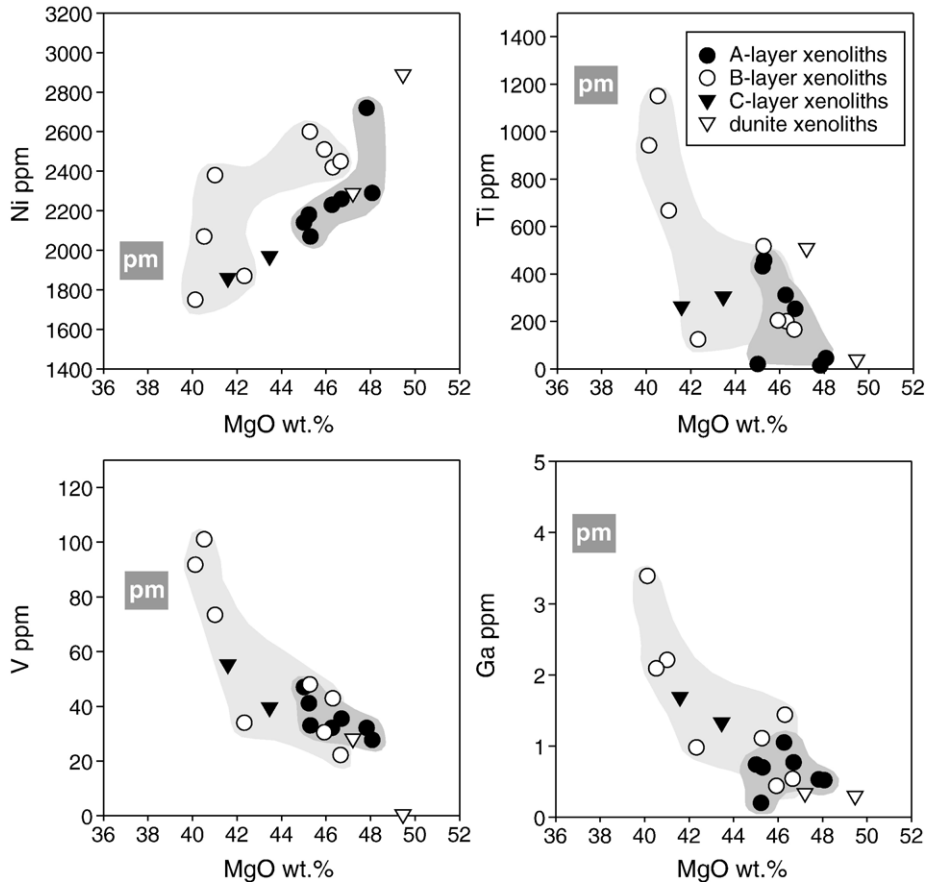

Fig. 4. Selected trace element plots for the Kaavi-Kuopio xenoliths. Moderately incompatible elements define good trends between the primitive mantle (McDonough and Sun, 1995) and the most depleted samples (dunites). In the Ni vs. MgO plot most B-layer samples have systematically higher Ni content at given MgO value compared to A- and C-layer samples.

7.3. Re–Os results

7.3.1. Rhenium abundances in peridotite xenoliths

Rhenium concentrations of Karelian peridotite samples cover a wide range extending from highly depleted values (0.026 ppb) to those that exceed the estimates of fertile mantle (0.28 ppb; McDonough and Sun, 1995). The average and median values are much higher than Re abundances reported for e.g. peridotites from the Kaapvaal cratonic root (e.g. Carlson et al., 1999). Rhenium content does not correlate with the indices of partial melting (such as Al_2O_3, MgO, Ti or Sc), but do show positive, if only rather weak, correlation with chemical indices of hydrous metasomatism (such as Rb, Sr, Ba, and LREE). Peltonen et al. (1999) suggested, that this metasomatism in Karelian samples was related to the introduction of kimberlite-like melt or fluid shortly before or during the emplacement. This is most likely source of the excess Re as well, since the high-Re samples may have Re–Os mantle model ages (T_{MA}) either negative or older than the age of the Earth. However, since the highest Re values for xenoliths are almost as high as that of the host kimberlite, the metasomatising media cannot simply be the kimberlite melt but more likely was a strongly fractionated fluid. Sulfur abundances of xenoliths, when available, are very low (2.2–13.9 ppm) compared to that of primitive mantle (250 ppm; McDonough and Sun, 1995). This implies that peridotites are strongly depleted residues, and Re was not added with a sulphur-rich fluid, but probably as Cl-complexes.

7.3.2. Osmium abundances in peridotite xenoliths

Osmium concentrations show some scatter, but most of the samples have values close to primitive mantle (Fig. 5). One outlier sample has abnormally high value of 13.19 ppb probably due to the nugget effect in these relatively small samples. In moderately depleted samples Os abundances first slightly increase, whereas higher degree of melt extraction seem to strongly

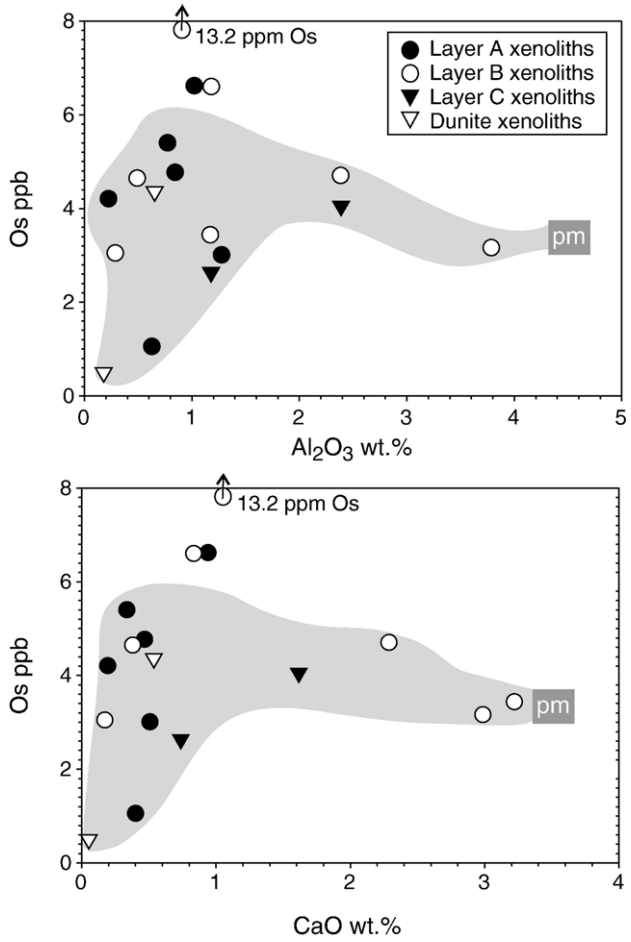

Fig. 5. Osmium abundances (ppb) vs. Al_2O_3 (wt.%) and CaO (wt.%) for the Kaavi-Kuopio xenoliths. Data are somewhat scattered but reveal the general trend of increasing Os in the residue at moderate degrees of partial melting, and rapid depletion at high degrees of mantle melting. This is consistent with Os abundances being controlled by variable degrees of partial melting in the presence of residual mantle sulphides.

deplete the peridotites in Os and the most depleted samples may contain only < 1 ppb osmium (Fig. 5). This behavior is consisted with Os abundances being controlled by residual sulphide. At moderate degrees of melting high $D(Os)_{sul/sil}$ value causes Os to be highly compatible but at higher degrees of melting this Os-rich sulphide phase finally became consumed and the residue becomes depleted in osmium.

7.3.3. Re–Os isotope systematics of peridotite xenoliths

With one exception, all our samples have $^{187}Os/^{188}Os$ less than that of fertile mantle suggesting that Re–Os system primarily records an ancient partial melting event of the peridotites (Fig. 6). In contrast to many other cratonic mantle xenolith suites (e.g. Carlson et al., 1999; Meisel et al., 2001; Pearson et al., 2004), the $^{187}Os/^{188}Os$ of Karelian samples show good general correlation with most indices of partial melting. Importantly, systematic differences are present between samples from the distinct mantle layers of A, B, and C (Fig. 7). Samples from layer B cover a wide compositional range and $^{187}Os/^{188}Os$ shows good correlations with moderately incompatible major elements. Samples from the most depleted layer A show distinct behaviour. At given content of moderately incompatible elements (Al, Ca, Ti, V, Sc, Ga) they have more radiogenic $^{187}Os/^{188}Os$ than samples from other layers. Because this shift is evident in the initial osmium isotopic ratios calculated at the time of the kimberlite eruption (600 Ma), it is not due to xenolith–kimberlite interaction, but is indicative that layer A has had distinct history compared to layer B. Layer A samples do not show any correlation with major or trace elements and the T_{RD} ages (as corrected to time of eruption) range between 1.34 and 2.57 Ga. The lower bound age is indicative that layer A includes also Archean protoliths

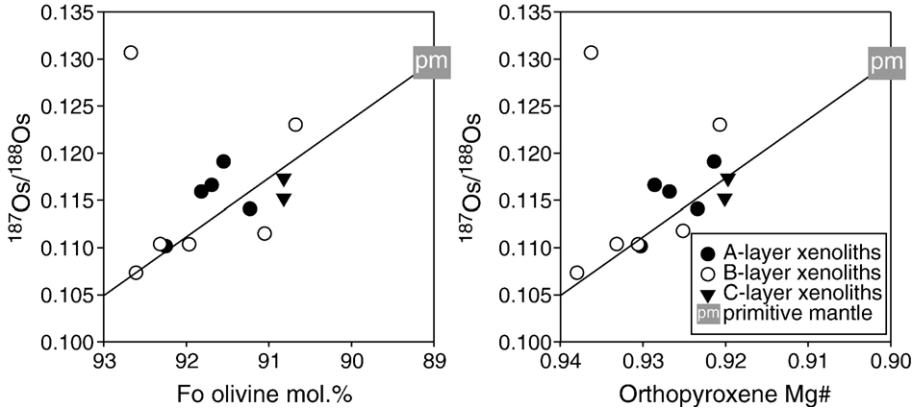

Fig. 6. Osmium isotopic composition of the Kaavi-Kuopio mantle xenoliths vs. Mg# of olivine and orthopyroxene. Layer B samples show large range of isotopic compositions and–with the exception of single samples–can be fitted to an "aluminachron". This suggests that layer B samples are related by an old melting event. Correlation line is fitted by eye.

but that it has been later metasomatised or mixed with Proterozoic mantle material. Layer C samples are in many respects intermediate between layer A and layer B samples. They are only moderately depleted and plot close to the regression line defined by layer B samples or record more radiogenic composition. T_{RD} values of 1.59 Ga and 1.88 Ga may be indicative of Proterozoic origin or reworking at that time.

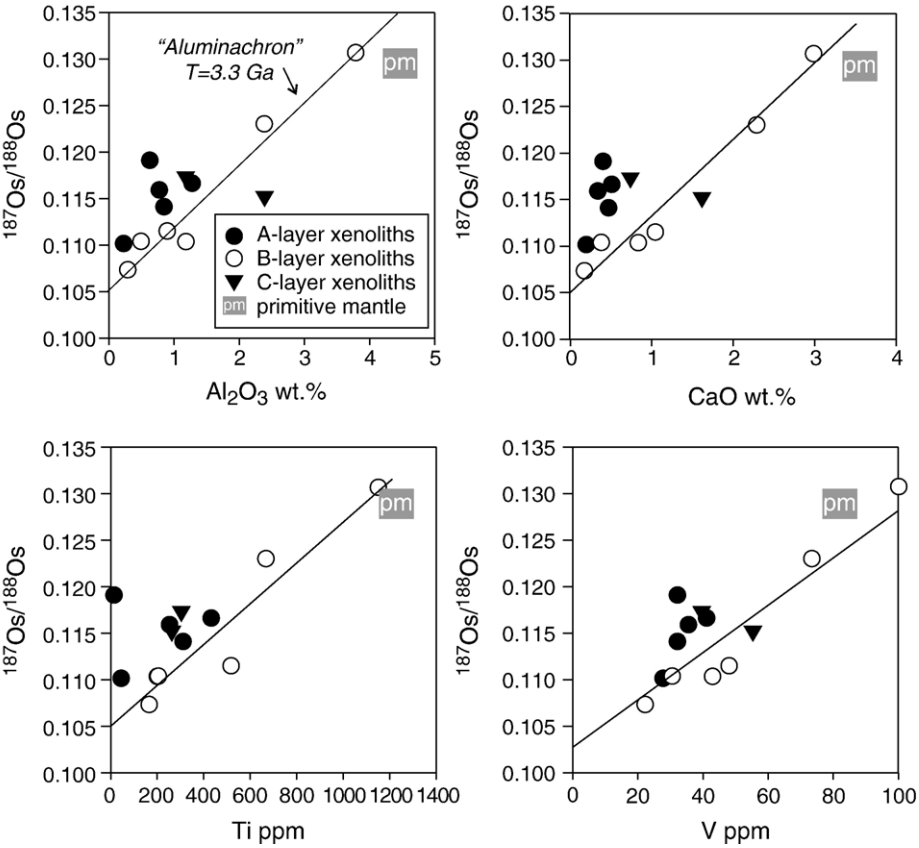

Fig. 7. Osmium isotopic composition of the Kaavi-Kuopio mantle xenoliths vs. abundances of moderately incompatible elements. Note the good correlation of the Layer B samples. Correlation lines–fitted by eye–intersect the ordinate at ~ 0.105 corresponding to an "aluminachron" age of ~ 3.3. Ga. Layer A samples have systematically more radiogenic compositions and plot above this "isochron".

7.3.4. Re–Os characteristics of kimberlites

Three kimberlite samples representing hypabyssal facies rocks from pipes #1, #2, and #14 yielded highly variable elemental abundances and Re–Os isotope ratios. Rhenium abundances of 0.185–0.969 ppb are relative high for kimberlites, but are within the total range reported in literature (Walker et al., 1989; Pearson et al., 1995a and 2003; Graham et al., 2004). Osmium contents of the three kimberlites analysed for Re–Os isotopes range from 0.218 to 0.840 ppb. These, too, are within the range reported for kimberlites, but are close to the lower limit reported for South African kimberlites (McDonald et al., 1995). Consequently, the Finnish pipes have high Re/Os. Osmium isotopic ratios of the kimberlites well exceeds that of primitive mantle and are radiogenic also when compared to most other kimberlites. Good correlation exists between $^{187}Re/^{188}Os$ and $^{187}Os/^{188}Os$, which rules out any post-emplacement mobility of rhenium, and is indicative of either time-integrated growth of radiogenic Os in high-Re/Os mantle source of kimberlites (cratonic mantle), or contamination of kimberlite magma with high $^{187}Re/^{188}Os$ and $^{187}Os/^{188}Os$ crustal material. Radiogenic Nd isotope composition ($\varepsilon Nd_{(600\ Ma)} = +0.8$) and unradiogenic Sr ($\varepsilon Sr_{(600\ Ma)} = -5.7$) (O'Brien and Tyni, 1999), however, are not indicative that extensive assimilation of granitic crust is the main source of radiogenic Os in kimberlites. A more plausible contaminant was sulphidic black schists that are ubiquitous within the early Proterozoic cover sequence that the kimberlites intruded. These black schists have high Re contents (25 ppb; Loukola-Ruskeeniemi, 1991) and are also characterised by highly radiogenic osmium isotopic compositions. Small amounts of black schist sulphides could explain the radiogenic osmium content of these samples that by other criteria are rather uncontaminated. Interestingly, xenoliths from the most contaminated kimberlite, i.e. pipe #2, with high $^{187}Os/^{188}Os$, do not have a more radiogenic Os composition than samples from other less contaminated pipes. This suggests that xenolith–kimberlite interaction mainly took place at subcrustal levels with no interaction with crustally contaminated kimberlite at later stages of eruption.

8. Discussion

The compositional layering of the Karelian craton lithosphere was first recognised by Peltonen et al. (1999) based on mantle xenoliths and was later mapped in more detail using garnet xenocrysts by Lehtonen et al. (2004). The origin of stratification has not been well understood. A first-rate constraint on the origin of the mantle layering at the Karelian Craton margin is provided by the garnet xenocryst data from another kimberlite locality far from the craton margin. O'Brien et al. (2003) reported that the whole mantle column in Kuhmo locality–some 150 km towards the core of the craton from Kaavi-Kuopio–consists of layer B-type lithosphere, and that layers A and C are absent in that area. This is strong evidence that the formation of strongly layered mantle, more specifically the origin of layers A and C, are somehow related to the (Paleoproterozoic) tectonic history of the western Karelian Craton margin, and not to Archean accretion by accumulating plume material or stacking of oceanic lithosphere.

8.1. Middle layer B—remnant of unmodified Archean continental mantle and the source of peridotitic diamonds

The middle layer B shares most of the characteristic features of the Archean continental mantle. First, it has abundant low Ca-high Cr harzburgitic garnets, believed to be a diagnostic of residual peridotites generated by high-degree mantle melting (komatiite extraction) during the Archean, i.e. garnet dunites and harzburgites. Good correlation of $^{187}Os/^{188}Os$ with indices of partial melting allow us to apply the "aluminachron" method of Reisberg and Lorand (1995), to derive the age for the melt extraction. Osmium isotopic composition vs. mildly incompatible element plots has regression lines that intercept the $^{187}Os/^{188}Os$ axis close to 0.105. This ratio corresponds to a T_{RD} age of ~3.3 Ga. This, together with the presence of harzburgitic "diamond indicator" garnets and diamondiferous nature of the kimberlites, are strong evidence that layer B is Paleoarchean in origin. The extrapolation method of Reisberg and Lorand (1995) has been criticised on the basis that Re may be consumed at a different stage of melting than Al_2O_3 and thus to give an erroneous model age (Pearson, 1999). This is, however, not critical to our conclusion because the compositional range of our samples extends close to Al- and Ca-free compositions, and also the maximum T_{RD} approaches 3 Ga.

The Archean origin of the layer B has important implications for the architecture of the lithosphere at the craton margin. The fact that the kimberlites intrude only some tens of kilometres in-craton from the Proterozoic–Archean boundary (Fig. 1) implies that this lithospheric boundary must be almost vertical to at least the base of the layer B, i.e. ~180 km. The protrusion of the Archean SCLM for some distance under the Proterozoic crust can not be ruled out, but the abrupt change in the neodymium isotopic composition of Proterozoic

granitic batholiths across this boundary excludes the presence of Archean crust west of this suture (Huhma, 1986). A comparable situation has been reported from the northeastern margin of the Tanzanian craton, where Archean lithospheric mantle has been preserved at least to the depth of 150 km, despite of the proximity of the intracontinental East African Rift (Lee and Rudnick, 1999).

The approximate "age" of depletion (~ 3.3 Ga) of the B-layer peridotites is comparable with the oldest formation ages of the overlying continental crust. Zircon crystallisation ages for TTG-series orthogneisses within the 3.0–3.5 Ga range have been reported from two localities near the western margin of the Karelian Craton (Paavola, 1986; Mutanen and Huhma, 2003). In addition, Peltonen et al. (in press) reported the presence of up to 3.5 Ga mafic granulites in the present lower crust at the kimberlite locality, and argued that the Karelian continental crust was up to 40–50 km thick already during the early Archean, and that upper and lower crust have remained coupled since that time, although being reworked during the Proterozoic. We believe that the matching U–Pb and Re–Os ages of upper crust, lower crust, and layer B peridotites, respectively, are not coincidental, but are indicative that layer B peridotites represent the ultimate source from which the oldest parts of the overlying continental crust were generated in the Archean. The almost exclusive restriction of diamond-indicator harzburgitic garnets within this ancient mantle layer is indicative of an Archean origin of peridotitic diamonds in Kaavi-Kuopio kimberlites.

8.2. Lower layer C—modification of the Archean cratonic root by Proterozoic rifting

Three features are of prime importance when constraining the origin of the lowermost layer C. (1) T_{RD} ages are Proterozoic (~ Svecofennian), (2) layer C is the primary source of TiO_2-, and Zr-rich garnets of typical megacryst composition and (3) even though harzburgitic "diamond indicator" garnets are absent, layer C still contains some highly depleted pyropes. Although the T_{RD} ages of the two C-layer samples are Proterozoic, they do not provide true age constraints. These samples are not sufficiently depleted to exclude an older age for melt extraction and, in fact, the $^{187}Os/^{188}Os$ vs. olivine and orthopyroxene compositional plots suggest that they are quite similar to B-layer samples (Fig. 6). An affinity with the B-layer-type mantle is also evident in some garnet xenocrysts. As shown in Fig. 2, C-layer pyropes contain on average more TiO_2 (and Zr and Y) than B-layer pyropes. However, also present are some very depleted pyropes—similar to those which tend to characterize Archean mantle. Recently, Lehtonen (2005) has reported that some C-layer pyrope xenocrysts have sinusoidal REE-patterns indicative of a two-stage evolution of the host peridotite: early extensive melt (komatiite?) extraction and later metasomatic overprinting. Importantly, these REE-patterns are nearly identical to those of B-layer pyropes strongly suggesting a similar genesis and history. Finally, since the C-layer seems to be the major source of megacrystic pyropes, we interpret that layer C represents layer B-type lithospheric mantle that has been refertilised by metasomatism. Zr–Y relationships of pyropes (Lehtonen et al., 2004) suggest that this metasomatism is more consistent with melt ingress than with fluid activity. The metasomatism was destructive to any harzburgitic garnets in this layer–as indicated by their abrupt disappearance across the boundary between layers B and C (Fig. 5)–and likely for any P-type diamonds in this layer as well. Since the presence of layer C is restricted to the craton margin (O'Brien et al., 2003) we relate its origin to the continental break-up at ~2 Ga due to plume impingement, as illustrated in Fig. 8.

8.3. Upper layer A—underthrusted Proterozoic arc wedge mantle?

Layer A has gone through a distinct evolution compared to layers B and C. The most striking feature is the "knife-sharp" boundary between layers A and B, as evident in the xenocryst data (Fig. 2), which is indicative of a sublithospheric shear zone. Several features distinguish layer A from the underlying layers: (1) peridotites indicate the high degree of melt depletion, (2) cryptic and modal phlogopite metasomatism are common, (3) garnets from this layer have an unusual composition (CCGE-garnets of Lehtonen et al., 2004, that are high in CaO, but extremely depleted in e.g. Ti, Zr, and REE), and (4) at a given degree of melt depletion, the Os isotopic composition is more radiogenic and highly variable if compared to layers B and C. Two distinct models can explain the Os isotopic composition of layer A samples. They may represent residues after extraction of a second stage melt from Archean protoliths. Since the analyses scatter and do not form any new "aluminachron" this would require that samples represent residues of several melting events of distinct age. Since such a series of successive melting events is not recorded in layer B this is considered unlikely. A more likely scenario involves metasomatism of the layer A. Radiogenic osmium isotopic composition

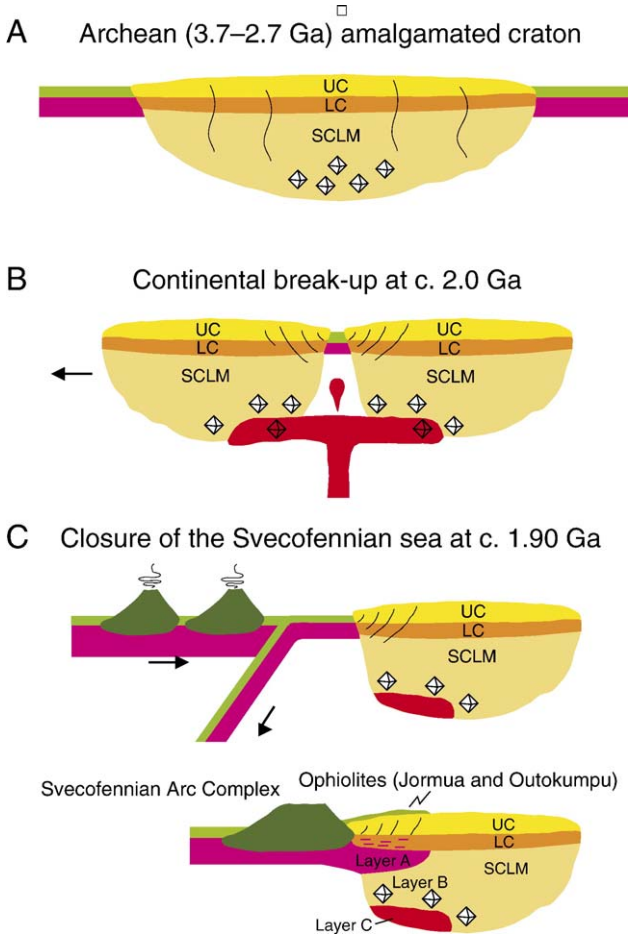

Fig. 8. Origin of the compositionally layered continental mantle at the Karelian craton margin. (A) Construction of the protocraton during Paleo- and Neoarchean times through accretion of microcontinents, island arcs and oceanic plateaus. Diamonds were probably formed within the thick cratonic roots already during Archean. (B) Continental, plume-induced, break-up stage at c. 2.0 Ga. Plume activity melt metasomatised the deepest levels of the continental mantle. This process was destructive to the Archean diamonds at the base of the lithosphere. Passive non-volcanic margin formed to the west of the Karelian craton and major ocean–the Svecofennian Sea–developed. (C) Closure of the Svecofennian Sea at c. 1.90 Ga due to westward subduction terminated by docking of the arc complex to the craton margin. This collision resulted in sandwiching of ultradepleted arc wedge mantle between crust and uppermost lithospheric mantle (origin of layer A). Layer B still represents the unmodified Archean continental mantle being the source of peridotitic diamonds in the Finnish kimberlites.

can be indicative of metasomatism. Since layer A is present only at the craton margin environment, we believe that it–like layer C–owes its unusual characteristics to the Proterozoic evolution of the craton margin. The maximum T_{RD} age of the layer A peridotites is 2.6 Ga (Table 3). This, together with the presence of (rare) harzburgitic garnets suggest that this layer contains remains of an Archean protoliths. Whether it consists only of reworked and metasomatised Archean peridotites or if significant proportion of "new" Proterozoic material has been tectonically thrusted beneath the craton margin cannot be resolved on the basis of osmium isotopes alone. Recent dating of the lower crust at the same locality provides additional constraints to the origin of the layer A. Peltonen et al. (in press) applied ion probe analyses to date zircons from xenoliths representing the mafic lower crust that overlies the mantle layer A. This crust appears to have a hybrid origin consisting of (1) up to 3.5 Ga old Archean mafic granulites and (2) Proterozoic amphibole-rich mafic granulites that mainly yielded formation ages of ~1.9 Ga. This age coincides with the amalgamation of the Svecofennian mobile belt to the craton margin. Hence, mantle layer A, too, is interpreted to have a complex origin consisting mainly of Proterozoic (Svecofennian) oceanic mantle underthrusted beneath the craton margin during the accretionary orogen (Fig. 8C). Small remnants of Archean SCLM–interleaved with imbricate

Table 3
Re–Os data for mantle xenolith and kimberlite whole rock samples, Kaavi-Kuopio kimberlites, eastern Finland

Sample no.	Lithology	Pipe no.	Layer	Depth	Re (ppb)	Os (ppb)	$^{187}Re/^{188}Os$	$^{187}Os/^{188}Os$ meas.	Error	$^{187}Os/^{188}Os$ (600)	γ Os (600)	TRD (Ga)[a]	TMA (Ga)
14.4/38.70	spi-harzburgite	14	A	c. 70	0.026	1.057	0.118	0.12030	0.00024	0.11911	− 3.1	1.34	1.63
14.7./66.65	spi harzburgite	14	A	c. 70	0.166	4.209	0.189	0.11206	0.00024	0.11016	− 10.4	2.57	4.09
9.2./24.37	gt-spi harzburgite	9	A	92	0.461	5.403	0.408	0.12003	0.00021	0.11593	− 5.7	1.78	25.82
14.4/30.55	gt-spi harzburgite	14	A	96	0.071	4.771	0.072	0.11483	0.00020	0.11412	− 7.2	2.03	2.31
Lu5-15-8/84.10	gt-spi harzburgite	5	A	103	0.088	3.011	0.141	0.11804	0.00023	0.11663	− 5.2	1.68	2.21
R18-38.45B	gt-spi harzburgite	2	B	113	0.174	6.601	0.126	0.11163	0.00018	0.11036	− 10.3	2.54	3.34
Lu5-15-4/37.80	gt-spi harzburgite	5	B	123	0.340	3.050	0.532	0.11269	0.00017	0.10734	− 12.7	2.95	− 9.61
R18-33.45	gt-lherzolite	2	B	147	0.400	13.190	0.145	0.11296	0.00018	0.11150	− 9.3	2.38	3.29
R18-38.45A	gt-lherzolite	2	B	150	0.356	4.704	0.362	0.12666	0.00022	0.12303	0.0	0.80	1.93
R18-37.05	gt-harzburgite	2	B	163	0.178	4.647	0.183	0.11223	0.00020	0.11039	− 10.2	2.54	3.96
Lu5-15-2/35.95	gt-lherzolite	5	B	164	0.761	3.165	1.155	0.14229	0.00040	0.13068	6.3	− 0.28	1.11
5.8./84.85	gt-lherzolite	5	C	206	0.397	4.054	0.469	0.11994	0.00021	0.11523	− 6.3	1.88	− 13.08
5.8./74	gt-harzburgite	5	C	234	0.025	2.636	0.046	0.11780	0.00023	0.11734	− 4.6	1.59	1.70
2.150/11.6	kimberlite	2			0.969	0.218	23.311	0.84575	0.00880	0.61157	397.3		1.85
14.05/39.05	kimberlite	14			0.548	0.840	3.143	0.17121	0.00030	0.13964	13.5	− 1.57	0.93
1.107/16.95	kimberlite	1			0.185	0.592	1.498	0.14055	0.00029	0.12550	2.1	0.45	0.66

[a] Corrected to time of eruption (600 Ma).

sheets of Proterozoic oceanic mantle–remain as expressed by presence of some harzburgitic garnets and old T_{RD} ages.

Chemical and isotopic features of the "ultradepleted" layer A peridotites are consistent with an arc mantle origin. They are highly depleted, cryptically and modally metasomatised olivine rich harzburgites. Their osmium isotopic composition, that is radiogenic at a given degree of partial melting compared to layer B samples, may be indicative of the infiltration of the layer A protoliths in the sub-arc mantle wedge by radiogenic slab-derived fluids and melts (Brandon et al., 1996; Widom et al., 2003). However, since there is no geological evidence for Proterozoic subduction towards northeast underneath the Karelian Craton margin, the ultradepleted harzburgites are interpreted to represent underthrusted Proterozoic arc lithosphere.

Although a vertical heterogeneity of cratonic lithosphere is rather common phenomena worldwide, sharply defined layering such as that observed across layers A and B is uncommon. It has been observed close to the Archean craton–Proterozoic mobile belt boundary in Greenland (Griffin et al., 2004) and within the Slave Craton, Canada, particularly in the central Slave domain where a "ultradepleted" layer similar to layer A in Karelia has been detected (Griffin et al., 1999; Menzies et al., 2004). The tectonic models proposed for these three localities suggest that sharp SCLM layering can have multiple origins. In Greenland, Proterozoic rocks were thrusted beneath older Archean SCLM (Griffin et al., 2004), but in the central Slave region the Archean "ultradepleted" layer became underplated by more fertile plume head material already during the Archean (Griffin et al., 1999). Yet the Karelian layered mantle seem to record a distinct origin: Paleoarchean Karelian SCLM (as presently represented by layer B) was first melt metasomatised at its base (origin of layer C) during a continental rifting at ~2.0 Ga, while its shallow parts (layer A) mainly consist of Proterozoic subduction wedge-type mantle that was underthrusted beneath the craton margin during continental collision between the craton and the Svecofennian island arc complex at ~1.9 Ga.

Acknowledgements

Dr H. Philip is thanked for help during the analytical work. This is a contribution from the GTK's (Geological Survey of Finland) *Geological and Metallogenic Modelling Study Group*. The manuscript benefited from reviews by Dr. D.G. Pearson and an anonymous referee.

References

Birck, J.L., Roy Barmann, M., Chapmas, F., 1997. Re–Os isotopic measurements at the femtomole level in natural samples. Geostandards Newsletters 20, 19–27.

Bogdanova, S.V., Gorbatschev, R., Garetsky, R.G., 2005. East European Craton. In: Selley, R.C., et al. (Ed.), Encyclopedia of Geology, vol. 2. Elsevier, Oxford, pp. 34–49.

Boyd, F.R., Pearson, D.G., Merzman, S.A., 1999. Spinel-facies peridotites from the Kaapvaal root. In: Curney, J.J., et al. (Ed.), Proc. 7th International Kimberlite Conference, Cape Town, vol. 1, pp. 40–48.

Brandon, A.D., Creaser, R.A., Shirey, S.B., Carlson, R.W., 1996. Osmium recycling in subduction zones. Science 271, 861–864.

Canil, D., 2004. Mildly incompatible elements in peridotites and the origins of mantle lithosphere. Lithos 77, 375–393.

Carlson, R.W., Pearson, D.G., Boyd, F.B., Shirey, S.R., Irvine, G., Menzies, A.H., Gurney, J.J., 1999. Re–Os systematics of lithospheric peridotites: implications for lithosphere formation and preservation. In: Curney, J.J., et al. (Ed.), Proc. 7th International Kimberlite Conference, Cape Town, vol. 1, pp. 99–108.

Carlson, R.W., Irving, A.J., Schulze, D.J., Hearn Jr., B.J., 2004. Timing of Precambrian melt depletion and Phanerozoic refertilisation events in the lithospheric mantle of the Wyoming Craton and the adjacent Central Plains Orogen. Lithos 77, 453–472.

Chesley, J.T., Rudnick, R.L., Lee, C.-T., 1999. Re–Os systematics of mantle xenoliths from the East African Rift: age, structure, and history of the Tanzanian craton. Geochimica et Cosmochimica Acta 63, 1203–1217.

Clement, C.R., 1982. A comparative geological study of some major kimberlite pipes in the Northern Cape and Orange Free State. PhD thesis, University of Cape Town.

Graham, S., Lambert, D., Shee, S., 2004. The petrogenesis of carbonatite, melnoite and kimberlite from the Eastern Goldfields Province, Yilgarn Craton. Lithos 76, 519–533.

Griffin, W.L., Doyle, B.J., Ryan, G.G., Pearson, N.J., O'Reilly, S.Y., Davies, R., Kivi, K., Van Acterbergh, E., Natapov, L.M., 1999. Layered mantle lithosphere in the Lac de Gras Area, Slave Craton: composition, structure and origin. Journal of Petrology 40, 705–727.

Griffin, W.L., O'Reilly, S.Y., Doyle, B.J., Pearson, N.J., Coopersmith, H., Kivi, K., Malkovets, V., Pokhilenko, N., 2004. Lithosphere mapping beneath the North American plate. Lithos 77, 873–922.

Huhma, H., 1986. Sm–Nd, U–Pb and Pb–Pb isotopic evidence for the origin of the early Proterozoic Svecokarelian crust in Finland. Geological Survey of Finland, Bulletin 337.

Irvine, G.J., Pearson, D.G., Kjarsgaard, B.J., Carlson, R.W., Kopylova, M.G., Dreibus, G., 2003. A Re–Os isotope and PGE study of kimberlite derived peridotite xenoliths from Sometset Island and a comparison to the Slave and Kaapvaal cratons. Lithos 71, 461–488.

Korsman, K., Korja, T., Pajunen, M., Virransalo, P., 1999. The GGT/SVEKA Transect: structure and evolution of the continental crust in the Palaeoproterozoic Svecofennian orogen in Finland. International Geology Review 41, 287–333.

Lee, C.-T., Rudnick, R.L., 1999. Compositionally stratified cratonic lithosphere—petrology and geochemistry of peridotite xenoliths from the Labait Volcano, Tanzania. In: Gurney, J.J., et al. (Ed.), Proceedings of the 7th International Kimberlite Conference, Red Roof Design, Cape Town, vol. 2, pp. 503–521.

Lehtonen, M., 2005. Rare earth element characteristics of pyrope grains from the Kaavi-Kuopio kimberlites and implications for mantle metasomatism. Bulletin of the Geological Society of Finland 76, 31–47.

Lehtonen, M., O'Brien, H.E., Peltonen, P., Johanson, B.S., Pakkanen, L.K., 2004. Layered mantle at the Karelian Craton margin: P–T of mantle xenocrysts and xenoliths from the Kaavi-Kuopio kimberlites, Finland. Lithos 77, 593–608.

Loukola-Ruskeeniemi, K., 1991. Geochemical evidence for the hydrothermal origin of sulphur, base metals and gold in Proterozoic metamophosed black shales, Kainuu and Outokumpu areas, Finland. Mineralium Deposita 26, 152–164.

Luukkonen, E.J., 1992. Late Archaean and early Proterozoic structural evolution in the Kuhmo-Suomussalmi terrain, eastern Finland. University of Turku, Sarja A: II. Biologica-Geographica-Geologica 78. 115 pp.

Meisel, T., Walker, R.J., Irving, A.J., Lorand, J.-P., 2001. Osmium isotopic composition of mantle xenoliths: a global perspective. Geochimica et Cosmochimica Acta 65, 1311–1323.

Menzies, A., Westerlund, K., Grütter, H., Gurney, J., Carlson, J., Fung, A., Nowicki, T., 2004. Peridotitic mantle xenoliths from the kimberlites on the Ekati diamond mine property, N.W.T., Canada: major element compositions and implications for the lithosphere beneath the central Slave craton. Lithos 77, 395–412.

Mutanen, T., Huhma, H., 2003. The 3.5 Ga Siurua trondhjemite gneiss in the Archean Pudasjärvi Granulite Belt, northern Finland. Bulletin of the Geological Society of Finland 75, 51–68.

Nironen, M., 1997. The Svecofennian orogen. Precambrian Research 86, 21–44.

O'Brien, H.E., Tyni, M., 1999. Mineralogy and geochemistry of kimberlites and related rocks from Finland. In: Gurney, J.J., et al. (Ed.), Proceedings of the 7th International Kimberlite Conference, vol. 2. University of Cape Town, Cape Town, South Africa, pp. 625–636.

O'Brien, H.E., Lehtonen, M., Spencer, R.G.S., Birnie, A., 2003. Lithospheric mantle in eastern Finland: a 250 km 3D transect. 8th Int. Kimberlite Conf.. Extended Abstract FLA 0261.

Olive, V., Ellam, R.M., Harte, B., 1997. A Re–Os study of ultramafic xenoliths from the Matsoku kimberlite. Earth and Planetary Science Letters 150, 129–140.

Paavola, J., 1986. A communication on the U–Pb and K–Ar age relations of the Archaean basement in the Lapinlahti-Varpaisjärvi area, Central Finland. Geological Survey of Finland, Bulletin 339, 7–15.

Pearson, D.G., 1999. The age of continental roots. Lithos 48, 171–194.

Pearson, D.G., Shirey, S.B., Carlson, R.W., Boyd, F.R., Pokhilenko, N. P., Shimizu, N., 1995a. Re–Os, Sm–Nd, and Rb–Sr isotope evidence for thick Archean lithospheric mantle beneath the Siberian craton modified by multistage metasomatism. Geochimica et Cosmochimica Acta 59, 959–977.

Pearson, D.G., Irvine, G.J., Carlson, R.W., Kopylova, M.G., Ionov, D. A., 2002. The development of lithospheric keels beneath the earliest continents: time constraints using PGE and Re–Os isotope systematics. In: Fowler, C.M.R., et al. (Ed.), The Early Earth: Physical, Chemical and Biological DevelopmentGeological Society, London, Spec. Publ., vol. 199, pp. 65–90.

Pearson, D.G., Nowell, G.M., Dowall, D.P., Kjarsgaard, B.A., Kopylova, M.G., Armstrong, J.A., 2003. The relative roles of lithosphere and convecting mantle in kimberlites from Slave Province, NWT: constraints from Re–Os isotopes and olivine population studies: 8th International Kimberlite Conference. Final Long Abstract 0269. 5 pp.

Pearson, D.G., Irvine, G.J., Ionov, D.A., Boyd, F.R., Dreibus, G.E., 2004. Re–Os isotope systematics and platinum group element

fractionation during mantle melt extraction: a study of massifs and xenolith peridotite suites. Chemical Geology 208, 29–59.

Peltonen, P., Huhma, H., Tyni, M., Shimizu, N., 1999. Garnet peridotite xenoliths from kimberlites of Finland: nature of the continental mantle at an Archaean craton–Proterozoic mobile belt transition. In: Gurney, J.J., et al. (Ed.), Proceedings of the 7th International Kimberlite Conference, Red Roof Design, Cape Town, vol. 2, pp. 664–676.

Peltonen, P., Kinnunen, K., Huhma, H., 2002. Petrology of two diamondiferous eclogite xenoliths from the Lahtojoki kimberlite pipe, eastern Finland. Lithos 63, 151–164.

Peltonen, P., Mänttäri, I., Huhma, H., Whitehouse, M.J., in press. Multi-stage origin of the lower crust of the Karelian Craton from 3.5 to 1.7 Ga based on isotopic ages of kimberlite-derived mafic granulite xenoliths. Precambrian Research.

Puchtel, I.S., Hofmann, A.W., Mezger, K., Jochum, K.P., Shchipansky, A.A., Samsonov, A.V., 1998. Oceanic plateau model for continental crustal growth in the Archean: a case study from the Kostomuksha greenstone belt, NW Baltic Shield. Earth and Planetary Science Letters 155, 57–74.

Puchtel, I.S., Hofmann, A.W., Amelin, Yu.V., Garbe-Schönberg, C.-D., Samsonov, A.V., Shchipansky, A.A., 1999. Combined mantle plume-island arc model for the formation of the 2.9 Ga Sumozero-Kenozero greenstone belt, SE Baltic Shield: isotope and trace element constraints. Geochimica et Cosmochimica Acta 63, 3579–3595.

Reisberg, L., Lorand, J.-P., 1995. Longevity of sub-continental mantle lithosphere from osmium isotope systematics in orogenic peridotite massifs. Nature 376, 159–162.

Robinson, B.W., Graham, J., 1992. Advance in electron microprobe trace element analysis. Journal of Computer-Assisted Microscopy 4, 263–265.

Ryan, C.G., Griffin, W.L., Pearson, N.J., 1996. Garnet geotherms: pressure–temperature data from Cr-pyrope garnet xenocrysts in volcanic rocks. Journal of Geophysical Research 101, 5611–5625.

Schulze, D.J., 2003. A classification scheme for mantle-derived garnets in kimberlite: a tool for investigating the mantle and exploring for diamonds. Lithos 71, 195–213.

Skiöld, T., Bogdanova, S., Gorbatschev, R., Bibikova, E., 2001. Timing of late Palaeoproterozoic metamorphism in the northern Belomoridian belt, White Sea region: conclusions from U–Pb isotopic data and P–T evidence. Bulletin of the Geological Society of Finland 73, 59–73.

Sorjonen-Ward, P., Luukkonen, E., 2005. Archean rocks. In: Lehtinen, M., et al. (Eds.), Precambrian Geology of Finland—key to the evolution of the Fennoscandian Shield. Elsevier, Amsterdam, pp. 19–99.

McDonough, W.F., Sun, S.-s., 1995. The composition of earth. Chemical Geology 120, 223–253.

Vuollo, J., 1994. Palaeoproterozoic basic igneous events in eastern Fennoscandian Shield between 2.45 Ga and 1.97 Ga, studied by means of mafic dyke swarms and ophiolites in Finland. Acta Universitatis Ouluensis. Series A. Scientiae Rerum Naturalium 250. 116 pp.

Walker, R.W., Carlson, R.W., Shirey, S.B., Boyd, F.R., 1989. Os, Sr, Nd, and Pb isotope systematics of southern African peridotite xenoliths: implications for the chemical evolution of subcontinental mantle. Geochimica et Cosmochimica Acta 53, 1583–1595.

Widom, E., Kepehinskas, P., Defant, P., 2003. The nature of metasomatism in the sub-arc mantle wedge; evidence from Re–Os isotopes in Kamchatka peridotite xenoliths. Chemical Geology 196, 283–306.